Experimental validation of resistive wall mode instability models for active magnetic feedback control

E. Saad, P.R. Brunsell

Division of Fusion Plasma Physics, School of Electrical Engineering and Computer Science, KTH Royal Institute of Technology,SE-10044 Stockholm, Sweden

Introduction

The advanced Tokamak scenario relevant for steady state operation, among the objectives of ITER, would, in the absence of plasma rotation [1], [2], require a conductive shell to stabilize the ideal MHD modes. However, with finite conductivity present in the conductive shell the appearance of another instability is possible, namely the resistive wall mode. Such an instability may be mitigated by a model based feedback control algorithm. One possibility is to use a black box control model determined by experimental system identification [3]. In this work the white box model is pursued and validated.

EXTRAP T2R

This study is carried out in the EXTRAP T2R device (R_0=1.24 m, a=0.183 m) of type Reversed Field Pinch (RFP) with comparable toroidal and poloidal magnetic field. EXTRAP T2R is equipped with a set of 4x32 actuator coils placed outside the shell and 4x64 sensors placed inside the shell. The configuration is denoted 2x32 and 2x64 for both coils and sensors since they are pair connected to remove the even poloidal component. Using the fact that EXTRAP T2R has a relatively high aspect ratio it is possible to approximate the toroidal geometry of EXTRAP T2R with cylindrical geometry. To validate the obtained theoretical models, for the RWM and vacuum, a number of experiments are performed with the intention of exciting the Fourier harmonics {m,n}={1,-32..31} with viewable spectrum n={-32..31} for 2x64 sensors. A comparison study is also performed for the case with 2x32 sensors for vacuum.

Theoretical models

The RFP equilibrium, parametrized with θ_0 ,α, χ, is calculated according [4] $\nabla x\overline{B_0} = \mu(r)\overline{B_0} + \frac{\mu_0\overline{B_0}x\nabla p}{B_0^2}$, $\frac{dp}{dr} = -\chi\frac{r}{2\mu_0}\left(\frac{\mu_0 B_0^2}{2B_\theta} - \frac{B_z}{r}\right)^2$ and $\mu(r) = \mu_0\frac{\overline{b}\cdot\overline{j}}{\overline{b}\cdot\overline{b}} = \frac{2\Theta_0}{a}\left(1-\left(\frac{r}{a}\right)^\alpha\right)$. The plasma model used in this work is the linearized ideal MHD model in cylindrical geometry, which results in the following two coupled ordinary differential equations [5], for the perturbation variables ξ_r and p^*,

$$\left(\rho\gamma_{mn}{}^2 + \frac{f^2}{\mu_0}\right)r\frac{d}{dr}(r\xi_r) = c_{11}r\xi_r + c_{12}p^* \text{ and } \left(\rho\gamma_{mn}{}^2 + \frac{f^2}{\mu_0}\right)r\frac{d}{dr}(p^*) = c_{21}r\xi_r - c_{11}p^*.$$

The thin shell dispersion relation for the resistive wall mode can be written for every {m, n} harmonic

[6] as $\gamma_{mn}\tau_w = \left[\frac{r}{b_r^{m,n}}\frac{d(rb_r^{m,n})}{dr}\right]_{r_{w-}}^{r_{w+}}$. The resistive wall mode growth rate, γ_{mn}, is obtained by solving the plasma equations with the constraint RWM dispersion equation. The experimental Fourier decomposed radial magnetic field may be compared with the theoretical time evolution without plasma (vacuum) and with plasma. For the case with only vacuum the time evolution of the radial magnetic field at the wall may be expressed according [7] $\tau_{mn}\frac{db_r^w}{dt} + b_r^w = b_r^{ext}$. This equation dictates the exponential settling with the rate $\sim -\frac{1}{\tau_{mn}}$ and $\tau_{mn} = -\tau_w I_m^{w\prime} K_m^{w\prime}(1 + (mR_0)^2(nr_w)^{-2})^{-1}$. The theoretical time evolution of the radial magnetic field at sensor position b_r^w obtained for the plasma case may be expressed according to $\tau_{mn}\frac{db_r^w}{dt} - \gamma_{mn}\tau_{mn}b_r^w = b_r^{ext}$

The experimental procedure

The experiment proceeds to apply a step coil current wave form to all actuators, Figure 1 left panel, with the objective to excite a given toroidal mode number n. The direct excitable mode numbers in this device are n={-16,…,15} and due to sideband [8] it is possible to excite higher order modal numbers. The signal from the sensor array may be Fourier decomposed according to the expansion $b_r^w(r,\theta,\varphi,t) = \sum_m \sum_n b_r^{w\mathrm{m},n}(r,t)e^{i(\mathrm{m}\theta+n\varphi)}$ for poloidal mode number m and toroidal mode number n. Figure 2 right panel, shows an obtained component (n=12) for experimental data. The data is postulated to follow an exponential function behaviour according to $b_r^w = C_1 + C_2 e^{C_3 t}$ when fitting the data to one mode. For the vacuum case the data is fitted for the applied perturbation (load case also named “excitation”) and when the perturbation is released (“deexcitation”). This is performed for m=1 poloidal modes with 2x32 and 2x64 sensors.

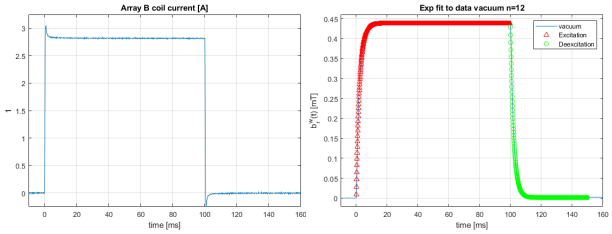

Figure 1 Left panel Step coil current wave form, Right panel: Exponential fit m=1 of received vacuum signal

$\Delta: C_3 = -470$

$o: C_3 = -479$

The experiment proceeds to validate the plasma-actuator response which are plotted in Figure 2 for toroidal mode n={-15,14, -11} that are examples of modes with different characteristics. These are plotted each for the case: without perturbation, with perturbation, vacuum case and the difference between the first two mentioned in reversed order [9]. The exponential fit is done for this difference due to field errors. Field errors occur due to

geometrical imperfections that resonate with the plasma and is modelled as an additive reproducible unknown magnetic field perturbation for EXTRAP T2R. The plasma response in Figure 2 left panel, is plotted for the toroidal mode n=-15 which is a resonant and initially stable mode and it can be seen that the magnetic field strength is larger compared to the vacuum case. The magnetic field rise time is different for the vacuum case and the plasma case. The rise time due to plasma has two distinct phases. The second unstable phase occur due the termination of plasma rotation. The plasma response for toroidal mode number n=14 is plotted in Figure 2 center panel. The toroidal mode number n=14 is a non-resonant stable mode and the magnetic field strength is lower than the only vacuum case during the plasma pulse discharge and after conforming to the vacuum case in steady state. The toroidal mode n=-11 is plotted, Figure 2 right panel, which is a non-resonant unstable mode. The plasma and the vacuum case may be fitted by exponential functions, Figure 3. The magnetic field averaged over the sensor area is a sum of odd modes m={1, -3, 5…} due to aliasing but the contribution from higher mode number is small. Thus the vacuum case is fitted by a sum of only m=1 and m=-3 modes. The vacuum case, for fitting two modes m=1, m=-3, the following fitting function is used $b_r^w = \frac{b_{vac}}{(1+r_{31})}\left((1-e^{C_1 t}) + r_{31}(1-e^{C_1 g_{31} t})\right)$, where b_{vac} is the vacuum steady state field. The parameters $g_{31} = \frac{\tau_{1n}}{\tau_{3n}}$ and $r_{31} = \frac{b_{3n}}{b_{1n}}$ are obtained from theoretical model of sensors and coils [9]. In the plasma case, for one mode m=1, the following fitting function is used $b_r^w = -\frac{b_{vac}}{(C_1)}\left(1 - e^{\frac{C_1}{\tau_{1n}} t}\right)$

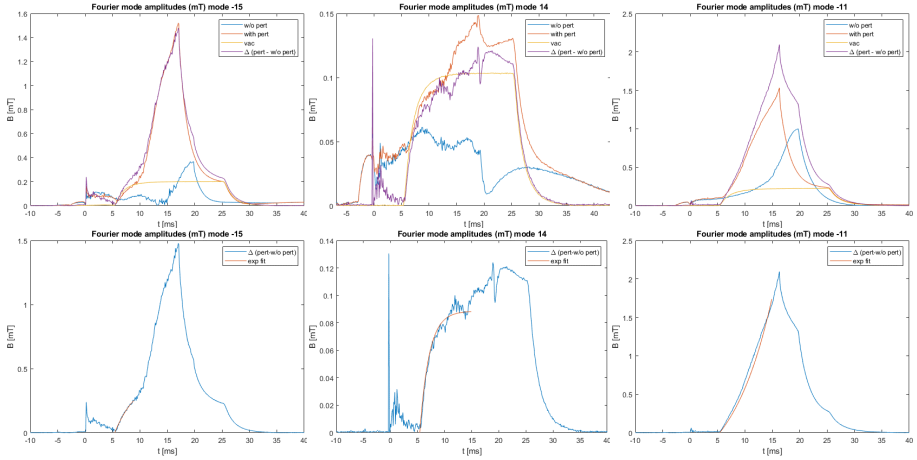

Figure 2 Amplitudes of n={-15,14-11} without perturbation, with perturbation, vacuum and Δ

Figure 3 Amplitudes of n={-15,14-11} with exponential fit for Δ

Results and Discussion

The results for the vacuum case are presented in Figure 4 a, Figure 4 b for 2x32 and 2x64. The theoretical curve is plotted for EXTRAP T2R parameters $r_w = 0.198m$, $\tau_w = 0.01s^{-1}$ for toroidal mode number n={-32,..,31}. The overall appearance of both data curves match in

the sense that the time constants decrease with higher modal number. This resembles the behavior of the theoretical curve τ_{mn}. The data curve 2x64 sensors produce better resemblance to the theoretical curve compared to 2x32 sensors. A plausible explanation of this discrepancy is aliasing in the toroidal direction. The time constants for two modal fitting of the vacuum case is presented in Figure 4 c for 2x64 sensors. The figure shows the theoretical curve of m=1 and m=-3 with the experimental obtained time constants τ_{mn}. The normalized growth rates obtained for the plasma discharge compared to the theoretical poloidal mode number m=1 is displayed in Figure 4 d. Equilibrium parameters, $\theta_0 = 1.65$, $\alpha = 3.8$, $\chi = 0$, toroidal magnetic field on axis 0.1 T and hydrogen plasma with particle density $5 \cdot 10^{18} m^{-3}$ was used to obtain the theory curve. The experimental data follows the theory curve for resonant modes -20<n<-11 while the experimental growth rates are higher for resonant modes n<-20. The deviation seen for n<-20 is generally expected for resonant modes due to resistive MHD effects not included in the present ideal MHD model. The agreement with the model for -20 < n < -11 is likely related to the screening effect of plasma rotation at the resonant surface delaying the resistive MHD response, and is observed only initially during the applied perturbation before the plasma rotation slows down [10].

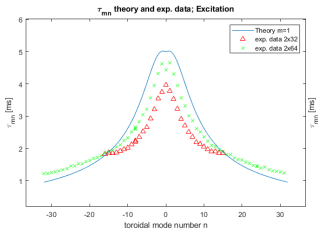

Figure 4 a τ_{mn} m=1 Excitation (Vacuo)

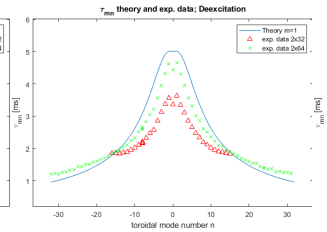

Figure 4 b τ_{mn} m=1 Deexcitation (Vacuo)

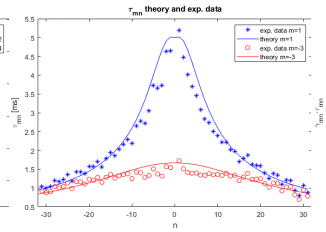

Figure 4 c τ_{mn} m={1,-3} (Vacuo)

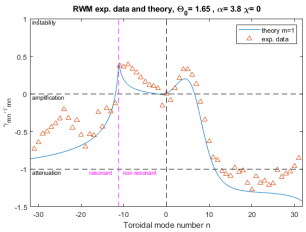

Figure 4 d $\gamma_{mn}\tau_{mn}$ m=1 (RWM).

Conclusion

The results presented for both the excitation and deexcitation in vacuum produce similar fits. 2x32 configuration gave a less close resemblance to the theoretical curve for both cases and the usage of the full sensor array produced almost the same as the theoretical curve. The theoretical RWM growth rates for the cylindrical linearized ideal MHD model has been compared to experimental data and are in reasonable agreement.

References

[1] Zheng L.J *et al.* (2010) Nucl. Fusion, **17**, 056104.
[2] V Igochine. (2012) Nucl. Fusion, **52**, 074010.
[3] K.Erik J. Olofsson et al (2013), Nucl. Fusion, **53**, 072003
[4] Z.R. Wang et al (2010), Physics of Plasmas, **17**, 052501
[5] G. Bateman (1978), MHD Instabilities, The MIT Press
[6] R. Fitzpatrick et al (1999), Physics of Plasmas, **6**, 3536
[7] K.Erik J. Olofsson (2010), KTH Thesis, ISBN: 978-91-7415-644-7
[8] PR Brunsell et al (2005), Plasma Phys. Control. Fusion, **47**,B25
[9] D. Gregoratto et al (2005), Physics of Plasmas, **12**, 092510
[10] L. Frassinetti et al (2012), 39:th EPS Conf. & 16 Int. Congress on Plasma Physics, P1.067